The Journal of Chemical Physics

Phase stability of colloidal mixtures of spheres and rods

Cite as: J. Chem. Phys. **154**, 204906 (2021); https://doi.org/10.1063/5.0048809
Submitted: 26 February 2021 . Accepted: 27 April 2021 . Published Online: 26 May 2021

J. Opdam, D. Guu, M. P. M. Schelling, D. G. A. L. Aarts, R. Tuinier, and M. P. Lettinga

The Journal of Chemical Physics ARTICLE scitation.org/journal/jcp

Phase stability of colloidal mixtures of spheres and rods

Cite as: J. Chem. Phys. 154, 204906 (2021); doi: 10.1063/5.0048809
Submitted: 26 February 2021 • Accepted: 27 April 2021 •
Published Online: 26 May 2021

J. Opdam,[1] D. Guu,[2] M. P. M. Schelling,[1] D. G. A. L. Aarts,[3,a)] R. Tuinier,[1,b)] and M. P. Lettinga[2,4,c)]

AFFILIATIONS

[1] Laboratory of Physical Chemistry, Department of Chemical Engineering and Chemistry, and Institute for Complex Molecular Systems (ICMS), Eindhoven University of Technology, P.O. Box 513, 5600 MB Eindhoven, The Netherlands
[2] Institute of Complex Systems, Forschungszentrum Jülich, D-52425 Jülich, Germany
[3] Department of Chemistry, Physical and Theoretical Chemistry Laboratory, University of Oxford, South Parks Road, Oxford OX1 3QZ, United Kingdom
[4] Laboratory for Soft Matter and Biophysics, KU Leuven, Celestijnenlaan 200D, B-3001 Leuven, Belgium

Note: This paper is part of the JCP Special Topic on Depletion Forces and Asakura–Oosawa Theory.
[a)] **Electronic mail:** dirk.aarts@chem.ox.ac.uk
[b)] **Electronic mail:** r.tuinier@tue.nl
[c)] **Author to whom correspondence should be addressed:** p.lettinga@fz-juelich.de

ABSTRACT

We determined the phase boundaries of aqueous mixtures containing colloidal rod-like *fd*-viruses and polystyrene spheres using diffusing-wave spectroscopy and compared the results with free volume theory predictions. Excluded volume interactions in mixtures of colloidal rods and spheres lead to mediated depletion interactions. The strength and range of this attractive interaction depend on the concentrations of the particles, the length L and diameter D of the rods, and the radius R of the spheres. At strong enough attraction, this depletion interaction leads to phase separation. We experimentally determined the rod and sphere concentrations where these phase transitions occur by systematically varying the size ratios L/R and D/R and the aspect ratio L/D. This was done by using spheres with different radii and modifying the effective diameter of the rods through either the ionic strength of the buffer or anchoring a polymeric brush to the surface of the rods. The observed phase transitions were from a binary fluid to a colloidal gas/liquid phase coexistence that occurred already at very low concentrations due to the depletion efficiency of highly anisotropic rods. The experimentally measured phase transitions were compared to phase boundaries obtained using free volume theory (FVT), a well established theory for calculating the phase behavior of colloidal particles mixed with depletants. We find good correspondence between the experimental phase transitions and the theoretical FVT model where the excluded volume of the rod-like depletants was explicitly accounted for in both the reservoir and the system.

I. INTRODUCTION

Entropy-driven ordering at the colloidal length scale has been well established[1] by theoretical,[2] simulation,[3,4] and experimental studies.[5–7] Colloidal particles that interact exclusively via hard body interactions offer relatively simple model systems for a statistical mechanical description. A higher degree of complexity can then be integrated into the simple models to take into account more intricate particle–particle interactions. Highly mono-disperse sterically stabilized spherical particles that mimic hard spheres can be synthesized in a laboratory by following well established protocols.[8,9] The phase behavior of such systems has been intensively studied, and transitions from liquid to crystalline and to jammed glassy states upon increasing sphere concentration have been observed.[7] The observed phase behavior can be explained by considering that at low volume fractions, maximum entropy is achieved in states having disordered particle configurations. As the volume fraction increases, the crystalline packing configuration facilitates more possible particle arrangements than the disordered states, and this, in turn, maximizes the entropy of the system. We thus have an ordering of a colloidal system that is purely driven by entropy.

Such entropy-driven phase transitions also occur in colloidal mixtures. Dispersions of colloids plus non-adsorbing polymers are a class of systems of which the phase behavior is well-studied.[10,11,12]

In such mixtures, the non-adsorbing polymer chains induce an effective attraction. This effective attraction between the spheres is indirectly caused by the repulsion between the colloidal surfaces and the non-adsorbing polymers, which leads to a zone that is depleted of polymers around the colloidal spheres. When the particles come close enough for their depletion zones to overlap, an unbalanced osmotic pressure mediated by the polymer chains results in an attractive force, which is called the depletion interaction. This polymer-mediated depletion interaction was first predicted by Asakura and Oosawa[13] and then further developed by Vrij;[14] it is discussed in detail elsewhere.[15] For certain compositions of colloidal mixtures, phase separation can lead to an increase in the free volume available to each species. Above a certain threshold concentration, the binodal, this increase in translation entropy is large enough to compensate the entropic cost of demixing and a phase transition will occur. The depletion induced attractive inter-particle force can lead to equilibrium phase behavior, analogous to molecular systems,[16] albeit richer.

Besides polymers, non-adsorbing colloidal particles can also be used to induce depletion forces. For this purpose, anisometric depletants are of special interest since they are highly efficient at mediating an attractive potential between the colloidal particles. This efficiency can be explained by considering the fact that the effective volume occupied by the depletants is much larger than the actual particle volume. Asakura and Oosawa already predicted in the 1950s[13,17] that for this reason, rod-like particles should be very efficient depletants. This efficiency has been confirmed experimentally with direct depletion potential measurements.[18–22] Moreover, due to the shape anisotropy of rods, rod/sphere mixtures have a very rich phase behavior. The topology of the phase diagram depends on two size ratios, namely, $\xi = L/R$ and $q = D/2R$, which are connected through the rod aspect ratio L/D. Here, L is the length of the rod, D is the diameter of the rod, and R is the radius of the colloidal spheres. Furthermore, rod-like particles can form ordered structures, i.e., liquid crystals and columnar phases, at high concentrations.[23–25]

Due to the richness of the phase behavior of rod/sphere mixtures, it is difficult to map the phase behavior as a function of particle concentrations for all the different parameters of interest. Some effort has been done in the literature to investigate regions of the phase stability map of rod/sphere mixtures. Bolhuis and Frenkel[26] studied the phase separation of colloidal spheres mixed with infinitely thin rods for different size ratios ξ with Monte Carlo simulations and perturbation theory. A strong effect of the size ratio on the phase behavior was found, and for size ratios above $\xi = 0.6$, an isostructural fluid/fluid coexistence region is present in the phase diagram. These results for infinitely thin rods were later corroborated by Schmidt[27] using density functional theory. A finite rod thickness can be taken into account with the relatively simple free volume theory (FVT), which has proven to provide many insights into the phase behavior of colloidal mixtures.[15] Vliegenthart and Lekkerkerker[28] used FVT to confirm the strong influence of ξ on the phase behavior of colloidal rod/sphere mixtures with finite thickness. Furthermore, they showed that the aspect ratio of the rods significantly affects the phase diagram through, for example, the location of the fluid/fluid critical point. Oversteegen and Roth[29] described a general method for FVT with anisotropic depletants using either scaled particle theory (SPT) or fundamental measure theory (FMT) to determine the free volume available for depletants. They used this FVT framework to study the phase behavior of spheres with rod-like depletants modeled as prolate ellipsoids and also found a strong influence on the thickness of the rods.

Experimental studies have also demonstrated the efficiency of rod-like depletants. Vliegenthart *et al.*[30] and Koenderink *et al.*[31] studied mixtures of boehmite rods and silica spheres with $\xi = 0.6$ and an aspect ratio of $L/D = 26$. They observed that beyond a certain rod concentration, the spherical particles phase separated into a colloidal fluid and a sphere-rich phase made up of crystallites. Oversteegen *et al.*[32] found similar results for boehmite rods mixed with silica spheres with $\xi = 0.3$ and an aspect ratio of $L/D = 8$. In both cases, the phase separation occurred already at very low rod and sphere concentrations as predicted by FVT. Yasarawan and van Duijneveldt[33] studied mixtures of sepiolite clay-rods and silica spheres with $\xi = 2.8$ and an aspect ratio of $L/D = 40$, where Bolhuis and Frenkel[26] predicted an isostructural fluid/fluid coexistence region. However, no fluid/fluid demixing was observed, which is likely because of the high concentration of rods in the samples that were already inside the isotropic/nematic coexistence gap. One disadvantage of these experimental systems was that the colloids were not density matched and each particle species sediments rather quickly, and therefore, gravity has an effect on the observed phenomena. To our knowledge, there is a dearth of systematic experimental studies in the literature on the bulk phase behavior in mixtures of colloidal rods and spheres. This might be due to the reason that there is a lack of model rods that are neutrally buoyant, having a narrow size distribution and a high aspect ratio. Although, recently a procedure to synthesize buoyant mono-disperse rods with a variable aspect ratio has been described.[34]

Another versatile colloidal rod-like model system that has been investigated[35–37] is the semi-flexible filamentous *fd*-virus. The viruses have an aspect ratio of ≈ 130 and are charge stabilized at values of pH > 4.2 due to the negative surface charge of the coat proteins.[38] In several studies, the *fd*-virus has been used to mediate an attraction between single spherical particles and a fixed wall and to determine the corresponding depletion potential.[18,20–22] The equilibrium phase behavior of mixtures of *fd*-viruses and polystyrene spheres has been investigated by Adams *et al.*[6] for size ratios ξ ranging from 6–80, obtained by using polystyrene spheres with different radii. In addition, in these experiments, the rod concentrations used were either close to the $I - N$ coexistence regime or were already at relatively high rod volume fractions where the rods self-assemble into highly ordered phases, and no fluid/fluid demixing was observed. Guu *et al.*[39] studied the effect of the rod thickness D on the phase behavior of *fd*-viruses and polystyrene spheres by varying the effective rod thickness through changing the ionic strength. The rod concentrations were much lower than in the experiments of Adams *et al.* and the size ratio used was $\xi = 3.5$. Guu *et al.* observed a transition from isotropic to an isostructural fluid/fluid coexistence upon increasing rod concentrations, as predicted by FVT calculations.[39] However, there was a big discrepancy between the onset of phase separation predicted by FVT and the experimental results. One of the reasons for this discrepancy is the fact that the used FVT method does not accurately account for the excluded volume of particle depletants.

In this paper, we will present a systematic study on the phase stability of colloidal rod/sphere mixtures consisting of *fd*-viruses

and density matched polystyrene spheres. We experimentally determined phase transition concentrations for size ratios $\xi = L/R$ ranging from 1.8 to 3.5. Moreover, we studied the effect of the thickness of the rods on the location of the phase boundary. This was done by altering the effective rod diameter through either changing the ionic strength of the buffer or covalently attaching short poly(ethylene glycol) (PEG) polymer chains onto the surface of *fd*-viruses. The experimental observations are compared with FVT results. To this end, we adjusted the original FVT approach to explicitly account for the excluded volume of the rod-like depletants in both the reservoir and the system, as done recently for hard-sphere depletants by Opdam *et al.*[40] The effective excluded volume of rods with a large aspect ratio is very large due to their anisotropic shape, and we will show that incorporating this excluded volume in FVT significantly improves the theoretical predictions with respect to the experimental results. The FVT model used in this paper is introduced in Sec. II. We present the description of the rod/sphere system and the experimental techniques used to determine the phase transition concentrations in Sec. III. Experimentally determined phase boundaries and the theoretical predictions are presented in Sec. IV, and the results are further discussed in Sec. V.

II. FREE VOLUME THEORY

Free volume theory[15,41] is a versatile tool used for the prediction of the phase behavior of colloidal systems interacting via depletion forces. Here, we outline the FVT method used in this paper, which is based on previous work on binary hard-sphere mixtures[40] but extended to take the anisotropic shape of rod-like depletants into account.

A. Semi-grand potential

In the FVT model, there are two compartments: the system of interest that contains colloidal particles and depletants and a hypothetical reservoir containing only depletants. These compartments are separated from each other through a membrane that is impermeable to the colloidal particles but is permeable to the depletants and the solvent, which is treated as a background in FVT. The two compartments are in osmotic equilibrium, and the thermodynamic properties of the system are described by the semi-grand potential. The experimental system of interest in this work is approximated as a mixture of colloidal hard spheres (s) and hard rod-like depletants (r) that only interact through excluded volume interactions. The rods are described as spherocylinders; i.e., cylinders with length L capped by hemispheres. The semi-grand potential of the system with a certain volume V and temperature T containing N_s spheres and N_r rods is defined as

$$\begin{aligned}\Omega(N_s, V, T, \mu_r) &= F_0(N_s, V, T) + \int_{-\infty}^{\mu_r} \left(\frac{\partial \Omega}{\partial \mu_r'}\right)_{N_s,V,T} \mathrm{d}\mu_r' \\ &= F_0(N_s, V, T) - \int_{-\infty}^{\mu_r} N_r(\mu_r')\, \mathrm{d}\mu_r', \end{aligned} \tag{1}$$

where μ_r is the chemical potential of the rods and $F_0(N_s, V, T)$ is the Helmholtz free energy of the colloidal hard-sphere system in the absence of rods. The number of rods in the system is not known *a priori* and depends on the number of rods in the reservoir and the number of spheres in the system. In order to obtain an expression for N_r, we will make use of the fact that the chemical potential μ_r is the same in both the reservoir and the system since both compartments are in osmotic equilibrium. Following Widom's insertion theorem,[42] an expression for μ_r can be written in terms of the work W needed to insert a rod into the system,

$$\mu_r = \text{const} + k_B T \ln \frac{N_r}{V} + W, \tag{2}$$

with k_B being the Boltzmann constant. For a system with only excluded volume interactions, the non-ideal contribution can be rewritten in terms of the free volume that is available in the system, resulting in

$$\mu_r = \text{const} + k_B T \ln \frac{N_r}{\langle V_{\text{free}} \rangle}, \tag{3}$$

where $\langle V_{\text{free}} \rangle$ is the ensemble averaged free volume. In previous FVT studies on mixtures of rods and spheres, the rods were treated as infinitely thin[26] or the chemical potential of the rods was assumed to be ideal and the volume that is excluded by the rod depletants themselves is neglected in the free volume expressions for both the reservoir and the system.[28,29,39] Here, we follow a FVT approach where the excluded volume of the rod-like depletants is explicitly accounted for, similar as was recently developed for binary hard-sphere mixtures.[40] Using this FVT method, Eq. (3) can still be applied to the chemical potential of the rods in the system; however, $\langle V_{\text{free}} \rangle$ has to be determined for the binary colloidal rod/sphere system. Moreover, Eq. (3) can also be applied to the chemical potential of the depletants in the reservoir but now with $\langle V_{\text{free}} \rangle$ determined for the reservoir containing only rods. Equating the chemical potentials of the rods in the system and the reservoir then gives the following expression for the number of rods in the system:

$$N_r = N_r^R \frac{\langle V_{\text{free}} \rangle^S}{\langle V_{\text{free}} \rangle^R}, \tag{4}$$

where the indications R and S refer to the reservoir and the system, respectively. A schematic representation of the equilibrium between the reservoir and the system is shown in Fig. 1. For convenience, we will use dimensionless quantities throughout the rest of this section, which are defined as

$$\begin{aligned} \widetilde{\Omega} &= \frac{\Omega\, V_s}{V\, k_B T}, \quad \widetilde{F} = \frac{F\, V_s}{V\, k_B T}, \quad \widetilde{\Pi} = \frac{\Pi\, V_s}{k_B T}, \\ \widetilde{\mu} &= \frac{\mu}{k_B T}, \quad \alpha = \frac{\langle V_{\text{free}} \rangle}{V}, \quad \phi_i = \frac{N_i V_i}{V}, \end{aligned} \tag{5}$$

where i denotes either component s or r, V_i is the volume of component i, Π is the osmotic pressure, and α is the free volume fraction. Using these definitions, Eqs. (1) and (4) are rewritten as

$$\widetilde{\Omega} = \widetilde{F}_0 - \frac{V_s}{V_r} \int_{-\infty}^{\widetilde{\mu}_r} \phi_r(\widetilde{\mu}_r')\, \mathrm{d}\widetilde{\mu}_r', \tag{6}$$

$$\phi_r = \phi_r^R \frac{\alpha^S(\phi_s, \phi_r)}{\alpha^R(\phi_r^R)}. \tag{7}$$

Combining Eqs. (6) and (7) and applying the Gibbs–Duhem equation,

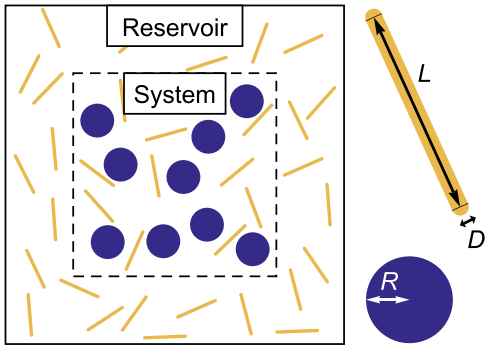

FIG. 1. Schematic representation of FVT. The dashed black line represents a semi-permeable membrane that cannot be passed by the colloidal spheres but is permeable to the rods and solvent. The size ratios $q = D/2R$ and $\xi = L/R$ in this scheme are 0.1 and 2.4, respectively, so the aspect ratio L/D equals 12.

$$\frac{V_s}{V_r}\phi_r^R \mathrm{d}\widetilde{\mu}_r = \mathrm{d}\widetilde{\Pi}^R, \tag{8}$$

gives the following result for the semi-grand potential:

$$\widetilde{\Omega}_k = \widetilde{F}_{0,k} - \int_0^{\phi_d^R} \frac{\alpha_k^S}{\alpha^R}\left(\frac{\partial\widetilde{\Pi}^R}{\partial\phi_d^{R'}}\right)\mathrm{d}\phi_d^{R'}. \tag{9}$$

Here, k denotes the phase state of the spherical particles, which is assumed to be either a fluid or a face-centered cubic (FCC) crystal. In this work, we focus on the isostructural fluid/fluid coexistence of the spherical colloids, which occurs at the low density region of the phase diagram. The free energy of the pure hard-sphere fluid can be approximated from the Carnahan–Starling equation of state,[43] resulting in

$$\widetilde{F}_{0,\mathrm{fluid}} = \phi_s\left[\ln\left(\phi_s\Lambda^3/V_s\right) - 1\right] + \frac{4\phi_s^2 - 3\phi_s^3}{(1-\phi_s)^2}, \tag{10}$$

where Λ is the de Broglie wavelength. For the range of reservoir concentrations used in this work, it is expected that the rod-like particles do not form a nematic phase but behave as a fluid.[23,44] Therefore, the scaled particle theory (SPT) result for a fluid dispersion of hard spherocylinders[45] is used for the osmotic pressure in the reservoir,

$$\widetilde{\Pi}^R = \frac{V_s}{V_r}\left[\frac{\phi_r^R}{1-\phi_r^R} + \frac{3\gamma(\gamma+1)}{3\gamma-1}\left(\frac{\phi_r^R}{1-\phi_r^R}\right)^2 + \frac{12\gamma^3}{(3\gamma-1)^2}\left(\frac{\phi_r^R}{1-\phi_r^R}\right)^3\right], \tag{11}$$

where the parameter γ is related to the aspect ratio of the rods,

$$\gamma = 1 + \frac{L}{D}, \tag{12}$$

with L and D being the length and diameter of the rods, respectively, as shown in Fig. 1. The only unknown quantities left in Eq. (9) are the free volume fractions available for the rods in the reservoir and in the system.

B. Free volume fraction

The free volume fraction in a colloidal system is related to the work W required to insert an extra particle into the system and is given by

$$\alpha = \exp\left(-\frac{W}{k_BT}\right). \tag{13}$$

A general procedure to determine the work of insertion for hard particles is through the use of scaled particle theory (SPT).[46] In the 1970s, Cotter *et al.* developed a scaled particle approach to describe the thermodynamic properties of a fluid of hard spherocylindrical rods.[45,47–49] SPT has also been used to describe the free volume available to a rod-like depletant in a dispersion of hard spheres.[28] Later, it was shown that the free volume available for anisotropic depletants in a dispersion of hard spheres can generally be described using SPT or fundamental measure theory (FMT), which, in general, leads to similar or more accurate results than SPT when compared to the numerical results available for some anisotropic depletants with certain shape parameters.[29] More recently, SPT was used to describe a mixture of hard spheres and hard spherocylinders.[50] The SPT results are applied here to describe the free volume fraction for rod-like depletants in a rod/sphere mixture. A concise derivation of SPT for mixtures of spheres and spherocylinders will be given in this section, but for a more elaborate derivation, the reader is referred to the original work.[50]

The work of inserting a spherocylinder with length λL and diameter νD in a system containing spheres and spherocylinders is determined for the limiting cases $\lambda \to 0$, $\nu \to 0$ and $\lambda \gg 1$, $\nu \gg 1$. The case of interest with $\lambda = 1$, $\nu = 1$ can then be determined by connecting the two limiting cases through a Taylor series

$$\frac{W(\lambda,\nu)}{k_BT} = w_{00} + w_{10} + w_{01} + w_{11} + w_{02} + \frac{W(\lambda >> 1,\ \nu >> 1)}{k_BT}, \tag{14}$$

where w_{pq} are the terms of the Taylor expansion given by

$$w_{pq} = \frac{1}{p!q!}\left[\frac{\partial^{p+q}}{\partial\lambda^p\partial\nu^q}\frac{W(\lambda\to 0,\ \nu\to 0)}{k_BT}\right]_{\lambda,\nu=0}\lambda^p\nu^q. \tag{15}$$

Higher order terms of the Taylor expansion are neglected and are assumed to be described by the limit of large particle insertion, given by the last term on the right-hand side of Eq. (14). In the limit of small particle insertion ($\lambda \to 0$, $\nu \to 0$), the depletion zones are infinitely thin and the work of insertion is simply given by

$$\frac{W(\lambda\to 0,\ \nu\to 0)}{k_BT} = -\ln\left(1 - \phi_s\frac{V_{\mathrm{excl}}^{s,r2}}{V_s} - \phi_r\frac{V_{\mathrm{excl}}^{r,r2}}{V_r}\right), \tag{16}$$

where $V_{\mathrm{excl}}^{s,r2}$ and $V_{\mathrm{excl}}^{r,r2}$ are the orientationally averaged excluded volumes of the spheres and the spherocylindrical rods with respect to the inserted rod denoted as r2. These excluded volumes can be written in terms of the volume V, the surface area A, and the integrated mean curvature c of all the particles involved[29] as given in Table I,

$$V_{\mathrm{excl}}^{s,r2} = V_s + V_{r2} + c_{r2}A_s + c_sA_{r2}, \tag{17}$$

$$V_{\mathrm{excl}}^{r,r2} = V_r + V_{r2} + c_{r2}A_r + c_rA_{r2}. \tag{18}$$

The last term on the right-hand side of Eq. (14) is determined by the work to create a cavity for the inserted particle and is

TABLE I. Volume V_i, surface area A_i, and integrated mean curvature c_i of component i. R is the radius of the spherical particles, D is the thickness of the rods, L is the length of the rods, and λ and ν are the scaling parameters.

i	V_i	A_i	c_i
s	$\frac{4\pi}{3}R^3$	$4\pi R^2$	R
r	$\frac{\pi}{6}D^3 + \frac{\pi}{4}D^2L$	$\pi D^2 + \pi DL$	$\frac{L}{4} + \frac{D}{2}$
r2	$\frac{\pi}{6}(\nu D)^3 + \frac{\pi}{4}(\nu D)^2(\lambda L)$	$\pi(\nu D)^2 + \pi(\nu D)(\lambda L)$	$\frac{\lambda L}{4} + \frac{\nu D}{2}$

therefore related to the osmotic pressure $\widetilde{\Pi}^{\mathrm{S}}$ of the binary mixture in the system,

$$\frac{W(\lambda \gg 1,\, \nu \gg 1)}{k_{\mathrm{B}}T} = \frac{V_{\mathrm{r2}}}{V_{\mathrm{S}}}\widetilde{\Pi}^{\mathrm{S}}. \tag{19}$$

Combining Eqs. (14)–(19) and solving for $\lambda = 1$ and $\nu = 1$ finally yields the work of inserting a hard spherocylinder in a binary mixture of hard spherocylinders and hard spheres with the total volume fraction $\phi = \phi_{\mathrm{s}} + \phi_{\mathrm{r}}$,

$$\frac{W(\lambda = 1, \nu = 1)}{k_{\mathrm{B}}T} = -\ln(1-\phi) + a_2\frac{\phi}{1-\phi} + b_2\left(\frac{\phi}{1-\phi}\right)^2 + \frac{V_{\mathrm{r}}}{V_{\mathrm{s}}}\widetilde{\Pi}^{\mathrm{S}}. \tag{20}$$

An expression for the osmotic pressure of the binary system $\widetilde{\Pi}_{\mathrm{S}}$ can also be obtained using scaled particle theory,[50] resulting in

$$\widetilde{\Pi}^{\mathrm{S}} = \left(\phi_{\mathrm{s}} + \frac{V_{\mathrm{s}}}{V_{\mathrm{r}}}\phi_{\mathrm{r}}\right)\left[1 + \frac{\phi}{1-\phi} + \frac{A_{1,2}}{2}\frac{\phi}{(1-\phi)^2} + \frac{B_{1,2}}{3}\frac{\phi^2}{(1-\phi)^3}\right]. \tag{21}$$

In Eqs. (20) and (21), the following coefficients are used:

$$a_1 = 6\frac{\phi_{\mathrm{s}}}{\phi} + \left[\frac{1}{q}\frac{6\gamma}{3\gamma-1} + \frac{1}{q^2}\frac{6\gamma}{3(\gamma+1)}\right]\frac{\phi_{\mathrm{r}}}{\phi}, \tag{22}$$

$$a_2 = \left[\frac{3}{4}\xi(1+2q) + 3q(1+q)\right]\frac{\phi_{\mathrm{s}}}{\phi} + \left[6 + \frac{6(\gamma-1)^2}{3\gamma-1}\right]\frac{\phi_{\mathrm{r}}}{\phi}, \tag{23}$$

$$A_{1,2} = a_1\frac{\phi_{\mathrm{s}}}{\phi_{\mathrm{s}} + \phi_{\mathrm{r}}\frac{V_{\mathrm{s}}}{V_{\mathrm{r}}}} + a_2\left(1 - \frac{\phi_{\mathrm{s}}}{\phi_{\mathrm{s}} + \phi_{\mathrm{r}}\frac{V_{\mathrm{s}}}{V_{\mathrm{r}}}}\right), \tag{24}$$

$$b_1 = \frac{1}{2}\left(3\frac{\phi_{\mathrm{s}}}{\phi} + \frac{1}{q}\frac{6\gamma}{3\gamma-1}\frac{\phi_{\mathrm{r}}}{\phi}\right)^2, \tag{25}$$

$$b_2 = \left[\left(\frac{3}{4}\xi + \frac{3}{2}q\right)\frac{\phi_{\mathrm{s}}}{\phi} + \left(\frac{3(2\gamma-1)}{3\gamma-1} + \frac{3(\gamma-1)^2}{3\gamma-1}\right)\frac{\phi_{\mathrm{r}}}{\phi}\right] \cdot\left(3q\frac{\phi_{\mathrm{s}}}{\phi} + \frac{6\gamma}{3\gamma-1}\frac{\phi_{\mathrm{r}}}{\phi}\right), \tag{26}$$

$$B_{1,2} = b_1\frac{\phi_{\mathrm{s}}}{\phi_{\mathrm{s}} + \phi_{\mathrm{r}}\frac{V_{\mathrm{s}}}{V_{\mathrm{r}}}} + b_2\left(1 - \frac{\phi_{\mathrm{s}}}{\phi_{\mathrm{s}} + \phi_{\mathrm{r}}\frac{V_{\mathrm{s}}}{V_{\mathrm{r}}}}\right), \tag{27}$$

where the two dimensionless parameters describing the size ratio between the spheres and the rods are defined as

$$q = \frac{D}{2R}, \quad \xi = \frac{L}{R}. \tag{28}$$

Combining Eqs. (20)–(28) with Eq. (13) finally provides the free volume fraction α for a rod-like depletant in a colloidal system containing rods and spheres. The same equations can be used to find the free volume fraction for depletants in the reservoir by taking $\phi_{\mathrm{s}} = 0$. Furthermore, it is noted that the osmotic pressure of the binary mixture given by Eq. (21) reduces to the osmotic pressure of a fluid dispersion of rods given by Eq. (11) when $\phi_{\mathrm{s}} = 0$. The model described here reduces to the original FVT for rod/sphere mixtures[28] by setting the volume fraction of rods in the reservoir and the system to zero in the expressions for the free volume fraction. The expressions derived in this section are only valid for the isotropic case; however, a similar approach can be followed for a nematic phase by accounting for the orientational distribution function of the rods.[50] Another condition for the expressions in this section is that the spherical particles form a fluid phase since the osmotic pressure of the binary system given by Eq. (21) no longer holds if the spheres order in a solid phase. Moreover, it has been shown for penetrable hard-sphere depletants that the SPT approach for the free volume fraction in the solid phase becomes less accurate at higher packing fractions.[51]

C. Phase coexistence calculations

Fluid/fluid binodals of the mixture of hard spheres and hard rods are determined through the equilibrium conditions

$$\widetilde{\mu}_{\mathrm{s}}^{\mathrm{G}} = \widetilde{\mu}_{\mathrm{s}}^{\mathrm{L}}, \tag{29}$$

$$\widetilde{\Pi}^{\mathrm{G}} = \widetilde{\Pi}^{\mathrm{L}}, \tag{30}$$

where the superscript G denotes the colloidal gas phase and the superscript L denotes the colloidal liquid phase. The chemical potential of the spheres and the osmotic pressure are related to the semi-grand potential given by Eq. (9),

$$\widetilde{\mu}_{\mathrm{s}} = \left(\frac{\partial\widetilde{\Omega}}{\partial\phi_{\mathrm{s}}}\right)_{\widetilde{\Pi}^{\mathrm{R}},V,T}, \tag{31}$$

$$\widetilde{\Pi} = \phi_{\mathrm{s}}\widetilde{\mu}_{\mathrm{s}} - \widetilde{\Omega}. \tag{32}$$

Fluid/fluid coexistence densities for specific size ratios q and ξ were determined by solving Eqs. (29) and (30) with a numerical scheme. First, the distribution of the rod-like depletants between the reservoir and the system is numerically determined by solving Eq. (7) for a range of reservoir volume fractions $\phi_{\mathrm{r}}^{\mathrm{R}}$. The resulting data are interpolated and used as input to determine $\widetilde{\Omega}$ for a given volume fraction of spherical particles ϕ_{s} and a given $\phi_{\mathrm{r}}^{\mathrm{R}}$. These steps are repeated for a range of sphere volume fractions, and again, interpolation was used to obtain $\widetilde{\Omega}$ as a function of ϕ_{s}, which is used as input for Eqs. (29)–(32). Binodals are finally obtained by repeating this scheme for different values of $\phi_{\mathrm{r}}^{\mathrm{R}}$, which can be converted to the volume fraction of rods in the system ϕ_{r} using Eq. (7). All calculations are done using Wolfram Mathematica 12.

III. SYSTEM DESCRIPTION AND EXPERIMENTAL TECHNIQUES

A. Preparing mixtures of polystyrene spheres and *fd*-viruses

The model system was chosen such that we could vary the size ratios $\xi = L/R$ and $q = D/2R$ between the sphere and the rod as well as the aspect ratio L/D. The size ratios were varied by using spheres with different radii, and the aspect ratio was varied by changing the effective diameter of the rods through modifying the interaction potential between the particles. As colloidal spheres we used polystyrene spheres purchased from Thermo Scientific with a refractive index of 1.58. As their density is 1.05 mg/ml, they can be made neutrally buoyant using a buffer with a suited D_2O/H_2O mixture. See Table II for the used sizes and corresponding polydispersities.

The spheres were concentrated by centrifugation and redispersed in a TRIS–HCl buffer at pH = 8.3. The ionic strength of the buffer was set by adding NaCl to reach a total ionic strength of 25 mM or 100 mM, which gives a Debye length $\kappa^{-1} \approx 2$ or 1 nm, respectively. The polystyrene spheres carry a negative surface charge due to ionizable sulfate groups. We determined the concentration of the polystyrene spheres by drying the spheres in a vacuum oven and then measuring the dry weight of particles.

The *fd*-viruses are highly mono-disperse (contour length of 0.88 μm and a diameter of 6.6 nm) due to the fact that *fd* essentially clones itself using the biological machinery of the host bacterial cells. As the persistence length is $l_p \approx 3.0$ μm, the *fd*-virus can be considered as a semi-flexible rod. The *fd*-virus was obtained following the protocol outlined by Sambrook *et al.*[52] The *fd* was dispersed in a 10 mM TRIS–HCl buffer at pH = 8.3 set at ionic strengths of 25 and 100 mM. The virus concentration is measured by UV–VIS using an empirically determined extinction coefficient[53] of 3.84 mg cm^{-2} at 269 nm. At a pH > 7 and the ionic strength at which *fd* was suspended, the rods carry an estimated linear charge density[54] of 10–20 e/nm. Due to the surface charge, the rods exhibit a long range soft repulsion superimposed on top of the hard body interactions. The electrostatic repulsion between the rods is given by

$$\frac{U_{el}(x)}{k_B T} = \frac{\Gamma e^{-\kappa(x-D)}}{\sin(\beta)}, \tag{33}$$

where x is the separation distance between two rods, Γ is a constant resulting from the solution of the Poisson–Boltzmann equation, β is the orientation of one rod with respect to another, and κ^{-1} represents the Debye length.[55] In theoretical descriptions of the phase behavior, *fd* can be described as a hard rod with an effective diameter D_{eff}, which is larger than the bare *fd* diameter of 6.6 nm due to the range of the electrostatic repulsion. We assume that the effective length of the rods and the effective radius of the spheres are not affected by the range of the electrostatic repulsion since the Debye length is very small compared to L and R. D_{eff} can be determined empirically from the plot of the isotropic-nematic coexistence concentrations vs the ionic strength. The resulting effective diameters are $D_{eff} \approx 14$ nm and 11 nm at a buffer ionic strength of 25 mM and 100 mM, respectively.[54,56] Given the molecular mass of the *fd*-virus of $1.64 \cdot 10^7$ g/M, the number density can be calculated and, combined with D_{eff} and the length L, also the volume fraction of rods ϕ_r.

The long ranged repulsion of the *fd*-virus can be suppressed by modifying the surface properties of the rods. This was done by covalently attaching short poly(ethylene glycol) (PEG) polymer chains onto the coat proteins of the virus.[57] In the protocol, the end-functionalized PEG is attached onto the N-terminal end of virus coat proteins. Since the PEG used is electrically neutral, the polymer-coated rods interact predominantly via the steric repulsion depending on the surface density coverage by the linear polymer chains and on the ionic strength of the buffer. At an ionic strength of 25 mM, the surface charges lie completely within the PEG chains and are thus shielded. The effective rod thickness D_{eff} is now determined by the radius of gyration R_g of the polymer coils attached on the surface of the rod. As in the uncoated *fd* case discussed above, D_{eff} can be obtained from the plot of isotropic-nematic coexistence concentrations, which gives $D_{eff} \approx 19$ nm.

We prepared state-points in the phase diagram by mixing the desired rod/sphere concentrations diluted from the respective stock solutions. Both *fd*-viruses and polystyrene spheres were dispersed in buffered H_2O/D_2O mixtures. The spheres remained stable in solution, and sealed samples of the micro-sphere stock solution did not show any sedimentation over a period of several months. The rod/sphere mixtures are highly turbid upon mixing due to a mismatch of the buffer refractive index ($n_{buffer} \approx 1.33$) compared to that of the polystyrene spheres ($n_{spheres} \approx 1.6$).

B. Experimental methodology

The stability of the *fd*/sphere dispersions was tested by diffusing-wave spectroscopy (DWS). DWS was used to determine the rod concentrations where clustering is first observed, exploiting the fact that this method is developed for application in dispersions where multiple scattering occurs. DWS also has the advantage that it is highly sensitive to small changes in the turbidity of the colloidal dispersion. DWS was performed in transmission geometry. A quartz cuvette of 1 mm optical path length containing the sample was illuminated by a Spectra-Physics BeamLok 2060-06S Argon ion laser at a wavelength of 514.5 nm, and the transmitted light through

TABLE II. Physical properties of the polystyrene particles used to vary the size ratio ξ in the rod/sphere mixtures. Refractive indices were measured at a laser wavelength of $\lambda = 589$ nm.

Catalog No.	3495A	3600A	3700A	4009A
Mean diameter	496 ± 8 nm	600 ± 9 nm	707 ± 9 nm	994 ± 10 nm
Density	1.05 g/cm^3	1.05 g/cm^3	1.05 g/cm^3	1.05 g/cm^3
Refraction index	1.58	1.58	1.58	1.58

the sample was captured by an optical fiber and detected by an ALV single photon avalanche diode. An ALV-6010/160 multiple-tau correlator was used to compute intensity correlation functions.

The samples were mounted into the setup, directly after homogenizing the mixture by vortexing. Correlation functions were measured every 30 s until the system reached steady state. In stable mixtures, i.e., mixtures in which no phase separation occurred, the measured correlation functions did not change in time. In the case of phase separating mixtures, the characteristic relaxation time of the measured correlation functions increased as the mixture phase separated. Representative time evolution plots of correlation functions measured during an experiment are shown in Fig. 2(a) in the case of a stable mixture and in Fig. 2(b) in the case of a demixing rod/sphere dispersion. In classical diffusing-wave spectroscopy,[58] one defines a photon transport mean free path l^*. l^* is used as a fitting parameter of the measured auto-correlation functions. In our case, this characteristic length is ill-defined since in phase separating mixtures, there is a large distribution of cluster sizes and the turbidity changes as a function of time. We therefore fit the measured correlation functions by a stretched exponential function, yielding a single relaxation time τ. In Fig. 2(c), we plot the fitted τ as a function of time for two mixtures. We observe a clear difference between a sample with $\phi_r = 0.0090$, for which τ remains stable, and a sample with $\phi_r = 0.0099$, for which τ immediately increases. Thus, the phase transition point lies between these two rod concentrations. All the experimental phase transitions measured here are liquid–liquid-like, as determined with confocal laser scanning microscopy in a similar fashion as discussed in a previous paper.[39]

IV. RESULTS

In this section, we compare the experimentally observed phase stability transitions to the theoretically determined binodals for varying size ratio ξ and effective rod thickness D_{eff}. For this purpose, we only show the part of the theoretical binodals related to the volume fractions that were experimentally investigated. The full binodals including the liquid branch and the critical points can be found in Appendix B.

A. Phase boundaries as a function of size ratio ξ

We first study the effect of the size ratio ξ on the location of the phase stability boundary, varying ξ from 1.8 to 3.5 at an effective ionic strength of 25 mM, as plotted in Fig. 3. The solid symbols represent the highest volume fraction of rods, ϕ_r, for which the mixture is stable, at a given ϕ_s. The open symbols represent the lowest ϕ_r measured where the system will phase separate. The solid curves are the results for the binodals as determined with the free volume theory discussed in Sec. II and the dashed lines show the binodals from original FVT of Vliegenthart and Lekkerkerker.[28] The location of the binodal line shifts to higher rod volume fractions ϕ_r as ξ increases, as was also observed for the experimental phase transition concentrations. This result also corroborates numerical calculations[59] and calculations that are exact up to first order in rod density[60,61] which show that the depth of the depletion potential decreases monotonically as ξ increases.

The experimental phase transition concentrations correspond reasonably well with the predictions using the D_{eff} as determined from the location of the isotropic-nematic coexistence concentration vs the effective buffer ionic strength.[56] The theoretical predictions slightly underestimate the depletion effect resulting in a binodal at higher concentrations. Original free volume theory shows the opposite trend and systematically underestimates the binodal concentrations. With increasing ξ we observe that the discrepancy between the experimental results and the theoretical predictions becomes slightly larger. The increase in the phase transition volume fraction of the rods at lower sphere volume fractions is captured more accurately by

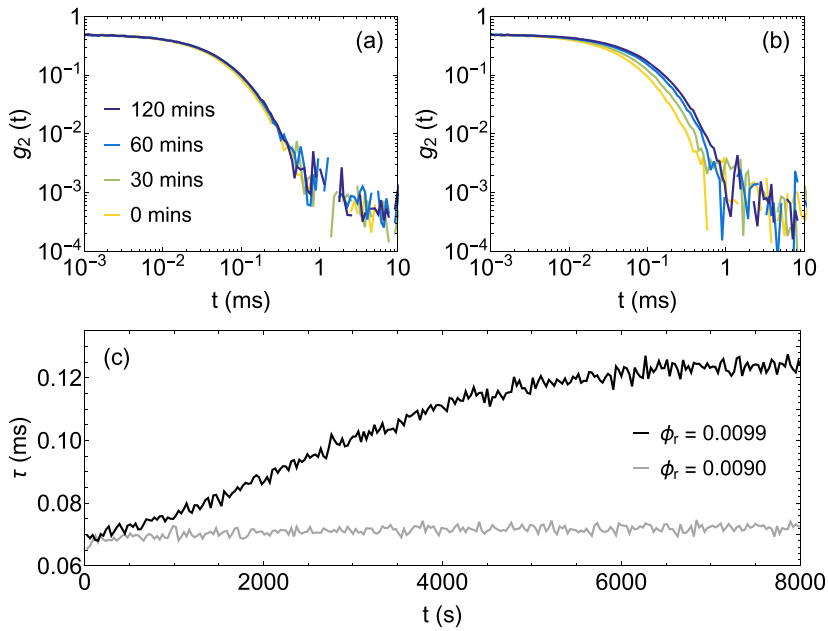

FIG. 2. Correlation functions from DWS experiments in a (a) stable mixture ($\phi_r = 0.0090$) and (b) unstable mixture ($\phi_r = 0.0099$) at a fixed sphere volume fraction of $\phi_s = 0.015$, taken at increasing times after mixing. (c) The mean relaxation time τ plotted as a function of time after quenching at the two indicated rod volume fractions ϕ_r. The increase in τ for $\phi_r = 0.0099$ is indicative for phase separation.

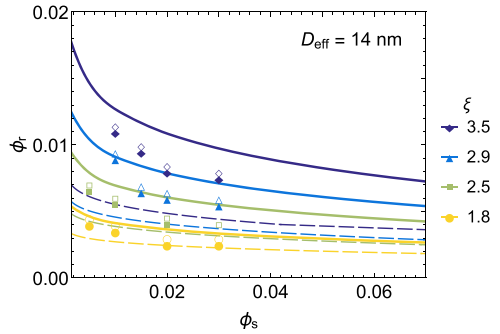

FIG. 3. Effect of size ratio ξ on the phase stability of colloidal rod/sphere mixtures. The symbols indicate the experimental phase transitions as determined from DWS measurements. The solid symbols denote the highest rod volume fraction ϕ_r at a fixed sphere volume fraction ϕ_s where the mixture was stable, while the open symbols indicate the lowest volume fraction of *fd* where the mixture was unstable. The radii of the spheres used in the experiments are 248 nm (purple), 300 nm (blue), 354 nm (green) and 497 nm (yellow) and the length of the *fd*-virus is 880 nm. The solid curves are binodals calculated using free volume theory where the excluded volume of the rod depletants is explicitly taken into account and the dashed curves show the results of original FVT for rod/sphere mixtures from Vliegenthart and Lekkerkerker.[28]

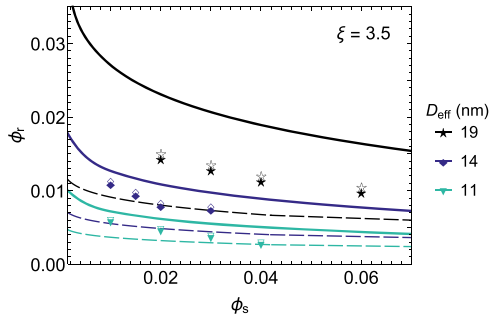

FIG. 4. Effect of the effective rod diameter on the phase stability of colloidal rod/sphere mixtures for a fixed ξ = 3.5. The symbols show the experimental results for effective diameters of $D_{eff} \approx 14$ nm (diamonds) and $D_{eff} \approx 11$ nm (triangles), obtained by using ionic strengths of 25 and 100 mM, respectively. The effective diameter of $D_{eff} \approx 19$ nm (stars) corresponds to the sterically stabilized *fd*-PEG complex at an effective ionic strength of 25 mM. The radii of the spheres used in the experiments are 248 nm, and the length of the *fd*-virus is 880 nm. The solid curves are binodals calculated using free volume theory where the excluded volume of the rod depletants is explicitly taken into account, and the dashed curves show the results of original FVT for rod/sphere mixtures from the work of Vliegenthart and Lekkerkerker.[28]

the new FVT and overall the deviation with the experimental results is less in comparison with the original FVT. In Appendix A we further discuss the differences between the FVT method from this paper and the FVT approach from Vliegenthart and Lekkerkerker.[28] We note here that we determined the fluid/fluid binodal with FVT, based on the observed phases in the experimental systems. At low sphere volume fractions the fluid/fluid region closes and the spheres are expected to phase separate into a fluid phase and a solid phase. The exact location of this transition was not investigated due to the lack of an accurate thermodynamic description of the binary solid phase.

B. Effect of rod thickness

In order to study the effect of the rod aspect ratio on the phase behavior, we tune the rod thickness D_{eff}. This can either be done by grafting the rod with a polymer layer or by changing the ionic strength of the buffer and thus the Debye length κ^{-1}. Here, we applied both approaches at a fixed ξ value of 3.5. Two buffers were prepared with the total ionic strengths set at 25 and 100 mM both at a pH of 8.3, yielding D_{eff} = 14 nm and D_{eff} = 11 nm, respectively. Figure 4 displays the phase transition volume fractions under the respective buffer conditions. The experimentally determined phase transitions were observed to shift to higher ϕ_r by a factor two as D_{eff} was increased from 11 to 14 nm, as shown in Fig. 4. This strong dependence of the location of the gas–liquid boundary on the rod aspect ratio is confirmed by the free volume theory calculations, and the effect of the difference in the rod thickness seems to be represented more accurately when the excluded volume of the rods is explicitly taken into account. The shift of the phase boundaries as a function of aspect ratio is also corroborated by calculations on the depletion potential[62] that showed that the depth of the attraction increases as a function of aspect ratio. These calculations involve a Derjaguin approximation for the pair potential. Although this is less accurate for $\xi > 1$ than the exact DFT approach,[61] it is expected that the observed trend is valid.

When comparing experiment and theory, one should keep in mind that *fd* and the polystyrene spheres are both negatively charged particles, which interact via a soft repulsive potential, while free volume theory assumes hard body interactions and does not consider the soft repulsive potential present in charged systems. In addition, we only took into account the increase of the rod diameter. The Debye length κ^{-1} for the charged polystyrene particles changes from ≈ 2 to 1 nm, which is less than 1% of the radius of the sphere. This small difference is not expected to significantly affect the location of the binodal.

Interactions are more hard-core-like when using polymer grafting to tune D_{eff}. With the polymer we used, the sterically stabilized rods have an effective diameter of D_{eff} = 19 nm. This system can directly be compared to the system at an ionic strength of 100 mM for which the surface charge is screened quite effectively so that it can also considered to be a hard rod system. The phase transition concentrations for the *fd*-PEG/sphere system are displayed in Fig. 4 and are further shifted toward higher ϕ_r, following the same trend as the charged system. The mismatch between the theoretical predictions and the experimental results seems to be significantly larger for the sterically stabilized rods compared to the rods with a soft electrostatic repulsion.

V. DISCUSSION

Free volume theory captures the observed phenomena semi-quantitatively, namely, the shift of the phase boundary to higher ϕ_r with an increasing size ratio ξ and decreasing aspect ratio of the rod. The predictions with closest agreement are for ξ = 1.8 in Fig. 3 and D_{eff} = 11 nm in Fig. 4, where the binodal volume fraction of the rods ϕ_r is small. In Fig. 5, we show the deviations of the experimentally measured rod volume fractions at the phase transition with respect to the binodal rod volume fractions $\phi_r^{t,VL}$ predicted by FVT of Vliegenthart and Lekkerkerker[28] for all the samples shown in

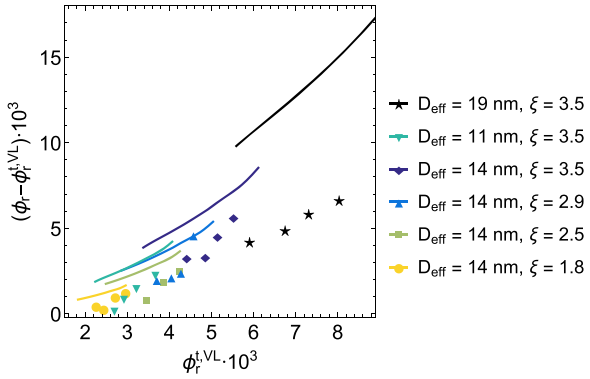

FIG. 5. Deviation of the experimental and FVT results with respect to the predictions from original FVT of Vliegenthart and Lekkerkerker.[28] The symbols denote the difference between the experimental phase transition rod volume fractions and the binodal rod volume fractions predicted by original FVT ($\phi_r^{t,VL}$) as a function of $\phi_r^{t,VL}$ for all the studied parameters ϕ_s, ξ, and D_{eff}. The color and shape of the symbols correspond to the data points in Figs. 3 and 4. The curves show the differences between binodal rod volume fractions predicted by FVT discussed in Sec. II and $\phi_r^{t,VL}$ as a function of $\phi_r^{t,VL}$ for the studied parameters ξ and D_{eff}, and ϕ_s ranging from 0.005 to 0.07.

Figs. 3 and 4. The experimental phase transition concentrations are taken as the average of the highest concentration where a stable mixture was found and the lowest concentration where phase separation occurs. We also show the deviation of the binodal rod volume fractions resulting from FVT discussed in Sec. II with the original predictions $\phi_r^{t,VL}$.

Figure 5 shows that there is an almost linear deviation between the experimental phase boundaries and the predictions of original FVT as a function of the binodal rod volume fraction for all the investigated samples. A similar linear deviation is also found when comparing the differences between the two FVT methods. This increasing deviation at higher rod volume fractions is most likely because the effect of the excluded volume of the rods is not accurately accounted for in the original theory, which becomes increasingly important at higher rod volume fractions. The fact that the deviations between the adjusted FVT and the experimental results with respect to original FVT show a similar trend indicates that explicitly taking the excluded volume of rods into account in the free volume descriptions of the reservoir and the system leads to a more accurate prediction of the phase stability.

Even though FVT captures the effects of ξ and D_{eff} on the phase stability of rod/sphere mixtures with reasonable accuracy, there is still a systematic overestimation of the binodal volume fractions compared to the experimental results. This is most likely due to inherent differences between the experimental model system and the theoretical model. Additionally, we compare differences between the experimental and theoretical phase transitions through the difference in the rod volume fraction at a certain sphere volume fraction. However, the experimental points show the rod volume fractions where colloidal clusters first start to form, whereas FVT gives the volume fraction where macroscopic phase coexistence occurs. A more detailed comparison could be obtained by measuring experimental tie-lines in macroscopically phase separated systems that can be directly compared with FVT results. This could also provide more insights into the location of the critical point in the experimental system. However, measuring such tie-lines is experimentally very involved.[63]

The *fd*-virus used in the experiments is semi-flexible, which is not accounted for in the current theory. Due to flexibility, the apparent length of the rods is shorter than the actual contour length,[18] leading to lower demixing volume fractions than expected for fully rigid rods. For colloid/polymer mixtures, it has also been shown that rigidity leads to binodals at higher depletant concentrations with FVT.[64] Furthermore, the rods and spheres are treated as mono-disperse in the calculations, whereas in the experiments, there is some polydispersity present. However, polydispersity of the colloidal spheres is not expected to have a large influence on the location of the fluid/fluid binodal.[65] Polydisperse depletants can lead to a lowering of the fluid/fluid binodal,[66,67] but the rod-like *fd*-virus used in the experimental system is very mono-disperse.

The *fd*-viruses used in the experiments are either electrostatically or sterically stabilized but are described as hard rods using an effective diameter based on the isotropic/nematic transition. With this approach, the softness of the repulsion between the charged rods is not fully accounted for. Moreover, the effective thickness is based on the electrostatic repulsion between the *fd*-viruses, but the repulsion between the *fd*-virus and the polystyrene spheres is different and therefore not properly accounted for in D_{eff}. Due to the high surface charge density of the *fd*-virus, the average effective thickness in the binary system is most likely smaller, which can explain the systematic over-prediction of the theoretical binodal concentrations. The difference in interactions can be taken into account in FVT by incorporating a different effective thickness of the rods for the excluded volume between the rods and the spheres than for the excluded volume between rods. The effect of the charges on the interactions between the polystyrene spheres is also neglected since the Debye length is very small compared to the sphere radius. However, this charge does affect the strength of the depletion potential of the spheres at close distances.

In the case of the sterically stabilized *fd*-PEG, the effective thickness is based on the interactions between rods, which all have a steric layer. The polystyrene spheres in the experiments do not have a steric polymer brush, and interactions between the PEG polymers on the *fd*-virus and the polystyrene surface might significantly affect the observed phase transitions. The interactions between PEG polymers and polystyrene particles have been studied in the literature, and in some cases, a bridging attraction between the polystyrene spheres caused by adsorbing PEG chains was observed.[68,69] Figure 5 clearly shows that the deviation between experiments and theory is significantly larger for the rods with steric stabilization than for the electrostatically stabilized rods. This might be because the PEG polymers on the surface of the *fd*-rods are not fully non-adsorbing but have some attraction with the surface of the polystyrene spheres. To verify this, the phases in the *fd*-PEG/polystyrene mixtures should be studied in more detail and more phase boundaries with *fd*-PEG depletants, for example, with varying PEG chain lengths, can be measured. Alternatively, PEG-stabilized colloidal spheres can be used to ensure steric repulsion between the surfaces of the spheres and the rods.

Finally, the deviation between experimental observations and FVT predictions seems to increase for larger size ratios ξ. This might be because the SPT approach used for the determination of the free volume becomes less accurate when the dimensions of the rod become large with respect to the spherical particles. SPT was used because an expression for the free volume available for a rod in a mixture of spheres and rods was readily available.[50] This description of the free volume might be slightly improved by using an FMT approach along the lines of Oversteegen and Roth;[29] however, the volume excluded by the rods has to be explicitly accounted for in the FMT expression. Despite the differences between the experimental system and the theoretical model, free volume theory seems to integrate the most important aspects and gives a reasonably accurate qualitative prediction of the phase boundaries for colloidal rod/sphere mixtures. For future work, the FVT method discussed throughout this paper can be used to further map the phase behavior of colloidal rod/sphere mixtures in a more complete parameter space.

VI. CONCLUSIONS

The effect of the sphere size and effective rod diameter on the phase boundaries of colloidal rod/sphere mixtures was systematically investigated with experiments and free volume theory. Phase transitions from isotropic to a fluid/fluid coexistence were observed in mixtures of polystyrene spheres and rod-like *fd*-viruses upon increasing the *fd* concentration. The size ratio $\xi = L/R$ between the rods and the spheres was varied by using chemically identical polystyrene spheres but with different diameters. The effective diameter D_{eff} of the charged *fd*-virus was varied by changing the ionic strength of the buffer or by attaching a short polymer brush to the surface of the rods. An increase in either ξ or D_{eff} results in a shift of the phase stability boundary toward higher rod volume fractions. These trends were confirmed by FVT calculations. The FVT model was extended to take the excluded volume of the rods explicitly into account in the descriptions of the free volume and the reservoir. The resulting theoretical predictions match the experimental measurements with reasonable accuracy. However, a systematic overestimation of the binodal concentrations was observed for the theoretical predictions compared to the experimental results. This is most likely due to the mapping of the experimental mixtures on the theoretical system of hard rigid particles using an effective rod diameter. The deviation between the experimental results and the FVT predictions was significantly larger for the sterically stabilized *fd*-PEG with respect to the electrostatically stabilized rods. This might be related to the interactions between the PEG brush on the *fd*-virus and the surface of the polystyrene spheres and requires further investigation.

ACKNOWLEDGMENTS

J.O. and R.T. acknowledge financial support from the Dutch Ministry of Economic Affairs of the Netherlands via the Top Consortium for Knowledge and Innovation (TKI) roadmap Chemistry of Advanced Materials (Grant No. CHEMIE.PGT.2018.006). D.G. acknowledges the International Helmholtz Research School of Biophysics and Soft Matter for financial support.

APPENDIX A: COMPARISON OF FVT METHODS

Figures 3 and 4 in Sec. IV showed the binodals determined with FVT of Vliegenthart and Lekkerkerker[28] and the binodals determined with FVT discussed in Sec. II where the excluded volume of the rods is explicitly taken into account. The main difference between the results of the two methods is that original FVT predicts the binodals at much lower volume fractions. In original FVT, the excluded volume of the rods is not accounted for in the free volume descriptions of the reservoir and the system. Therefore, the free volume available in the reservoir and the system is significantly higher than in reality. Moreover, the distribution of rods over the system and reservoir is no longer linear as a function of reservoir concentration when the excluded volume of the rods is taken into account. This is due to the possibility of overlap between the depletion zones around the rods and the depletion zones of the spherical particles or other rods. Because of this, the free volume fraction in the system decreases faster in the reservoir than in the system as a function of reservoir volume fraction ϕ_r^R. As a result, the volume fraction of rods in the system at a certain reservoir concentration is larger with respect to original FVT and the binodals shift toward higher rod concentrations.

The increase in rod concentrations in the system is demonstrated in Fig. 6 where the ratio between the volume fractions in the reservoir and in the system is plotted as a function of the volume fraction of rods in the reservoir for the values of ξ and D_{eff} of the studied rod/sphere mixtures. The ratio between the two volume fractions is given by the ratio of the free volume available in the reservoir and the system according to Eq. (7). The deviation between the two FVT methods is the largest for the highest size ratio ξ, which is expected since the size of the depletion zones are larger relative to the size of the spherical particles, and the effect of the excluded volume of the rods will be the strongest. The thickness of the rods does not have a strong influence on the deviation between the two FVT methods. The deviation in the binodals and in the depletant distribution between the two FVT methods is quite substantial, which is due to the fact that rod-like particles have a very large effective excluded volume relative to their physical volume. To further test the accuracy

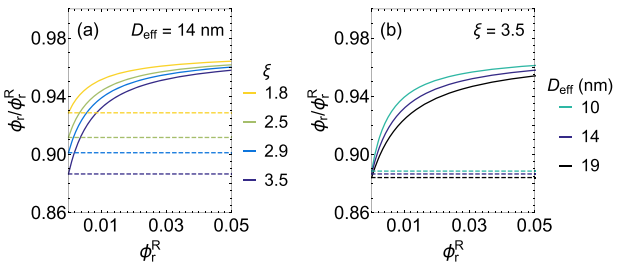

FIG. 6. The ratio of the rod volume fractions in the system and in the reservoir ϕ_r/ϕ_r^R as a function of the volume fraction of rods in the reservoir ϕ_r^R. The solid curves show the results of FVT in Sec. II, whereas the dashed lines show the results from the FVT method of Vliegenthart and Lekkerkerker.[28] The volume fraction of spheres is kept constant: $\phi_s = 0.03$. The length of the rods is 880 nm, and the radii of the spheres are 248 nm (purple), 300 nm (blue), 354 nm (green), and 497 nm (yellow) in (a) and 248 nm in (b), corresponding to Figs. 3 and 4, respectively.

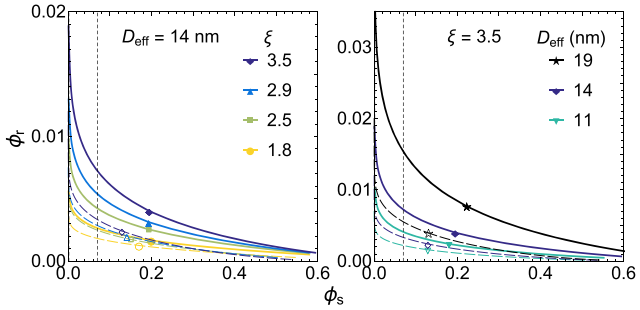

FIG. 7. Full FVT binodals of the rod/sphere mixtures discussed in Sec. IV. The solid curves are fluid/fluid binodals calculated using free volume theory where the excluded volume of the rod depletants is explicitly taken into account, and the dashed curves show the results of original FVT for rod/sphere mixtures from the work of Vliegenthart and Lekkerkerker.[28] The closed symbols indicate the critical point of the solid binodals, and the open symbols indicate the critical point of the dashed binodals. The vertical dashed lines indicate the region of the binodals that is shown in Figs. 3 and 4 ($0.0015 \leq \phi_s \leq 0.07$). Panel (a) shows the effect of the size ratio ξ on the binodal, and panel (b) shows the effect of the effective rod thickness D_{eff}.

of the FVT method, it would be interesting to compare the distribution of rods over the reservoir and the system, as shown in Fig. 6, with computer simulations. This distribution is fully determined by the free volume available in the system and in the reservoir through Eq. (7). Although these simulations have been performed for spherical depletants[70] and infinitely thin rods,[26] they have not been done for rods with a finite thickness.

APPENDIX B: FVT BINODALS

The full binodals of the studied rod/sphere mixtures, including the liquid branches and critical points, determined with FVT are shown in Fig. 7. The region that is shown in Figs. 3 and 4 in Sec. IV is indicated by the vertical dashed lines. We show both the results from FVT outlined in Sec. II (solid curves) and the original FVT approach of Vliegenthart and Lekkerkerker.[28] The critical points are estimated from the volume fractions where the gas branch and the liquid branch of the binodals meet. We emphasize that parts of the shown binodals are expected to be meta-stable with respect to the fluid/solid coexistence of the spherical particles since the binodals shown go up to sphere volume fractions larger than $\phi_s = 0.5$ where fluid/solid coexistence occurs for a pure hard-sphere dispersion. Mapping the full phase diagram of colloidal rod/sphere mixtures is beyond the scope of this work where we focus on the stability boundaries through the fluid/fluid binodals.

DATA AVAILABILITY

The data that support the findings of this study are available from the corresponding author upon reasonable request.

REFERENCES

[1] D. Frenkel, Physica A **263**, 26 (1999).
[2] L. Onsager, Ann. N. Y. Acad. Sci. **51**, 627 (1949).
[3] B. J. Alder and T. E. Wainwright, J. Chem. Phys. **27**, 1208 (1957).
[4] W. G. Hoover and F. H. Ree, J. Chem. Phys. **49**, 3609 (1968).
[5] S. Fraden, *Observation, Prediction, and Simulation of Phase Transitions in Complex Fluids*, NATO ASI Series C (Springer, 1995), Vol. 460, pp. 113–164.
[6] M. Adams, Z. Dogic, S. L. Keller, and S. Fraden, Nature **393**, 349 (1998).
[7] P. N. Pusey and W. van Megen, Nature **320**, 340 (1986).
[8] A. K. van Helden, J. W. Jansen, and A. Vrij, J. Colloid Interface Sci. **81**, 354 (1981).
[9] W. Stöber, A. Fink, and E. Bohn, J. Colloid Interface Sci. **26**, 62 (1968).
[10] W. C. K. Poon, J. Phys.: Condens. Matter **14**, R859 (2002).
[11] S. M. Ilett, A. Orrock, W. C. K. Poon, and P. N. Pusey, Phys. Rev. E **51**, 1344 (1995).
[12] A. P. Gast, C. K. Hall, and W. B. Russel, Faraday Discuss. Chem. Soc. **76**, 189 (1983).
[13] S. Asakura and F. Oosawa, J. Chem. Phys. **22**, 1255 (1954).
[14] A. Vrij, Pure Appl. Chem. **48**, 471 (1976).
[15] H. N. W. Lekkerkerker and R. Tuinier, *Colloids and the Depletion Interaction*, 1st ed. (Springer, 2011).
[16] W. Poon, Science **304**, 830 (2004).
[17] S. Asakura and F. Oosawa, J. Polym. Sci. **33**, 183 (1958).
[18] K.-h. Lin, J. C. Crocker, A. C. Zeri, and A. G. Yodh, Phys. Rev. Lett. **87**, 088301 (2001).
[19] L. Helden, R. Roth, G. H. Koenderink, P. Leiderer, and C. Bechinger, Phys. Rev. Lett. **90**, 048301 (2003).
[20] P. Holmqvist, D. Kleshchanok, and P. R. Lang, Eur. Phys. J. E **26**, 177 (2008).
[21] C. July and P. R. Lang, Langmuir **26**, 18647 (2010).
[22] S. De Sio and P. R. Lang, Z. Phys. Chem. **229**, 1161 (2015).
[23] P. Bolhuis and D. Frenkel, J. Chem. Phys. **106**, 666 (1997).
[24] S. V. Savenko and M. Dijkstra, J. Chem. Phys. **124**, 234902 (2006).
[25] V. F. D. Peters, M. Vis, Á. González García, H. H. Wensink, and R. Tuinier, Phys. Rev. Lett. **125**, 127803 (2020).
[26] P. Bolhuis and D. Frenkel, J. Chem. Phys. **101**, 9869 (1994).
[27] M. Schmidt, Phys. Rev. E **63**, 050201(R) (2001).
[28] G. A. Vliegenthart and H. N. W. Lekkerkerker, J. Chem. Phys. **111**, 4153 (1999).
[29] S. M. Oversteegen and R. Roth, J. Chem. Phys. **122**, 214502 (2005).
[30] G. A. Vliegenthart, A. van Blaaderen, and H. N. W. Lekkerkerker, Faraday Discuss. **112**, 173 (1999).
[31] G. H. Koenderink, G. A. Vliegenthart, S. G. J. M. Kluijtmans, A. van Blaaderen, A. P. Philipse, and H. N. W. Lekkerkerker, Langmuir **15**, 4693 (1999).
[32] S. M. Oversteegen, J. G. E. J. Wijnhoven, C. Vonk, and H. N. W. Lekkerkerker, J. Phys. Chem. B **108**, 18158 (2004).
[33] N. Yasarawan and J. S. van Duijneveldt, Soft Matter **6**, 353 (2010).
[34] C. Fernández-Rico, T. Yanagishima, A. Curran, D. G. A. L. Aarts, and R. P. A. Dullens, Adv. Mater. **31**, 1807514 (2019).
[35] S. Fraden, G. Maret, D. L. D. Caspar, and R. B. Meyer, Phys. Rev. Lett. **63**, 2068 (1989).
[36] Z. Dogic and S. Fraden, Curr. Opin. Colloid Interface Sci. **11**, 47 (2006).
[37] Z. Dogic and S. Fraden, *Phase Behavior of Virus/Sphere Mixtures and Entropy Driven Ordering within the Second Virial Approximation, Soft Matter* (Wiley-VCH Verlag GmbH & Co, 2005).
[38] K. Zimmermann, H. Hagedorn, C. C. Heuck, M. Hinrichsen, and H. Ludwig, J. Biol. Chem. **261**, 1653 (1986).
[39] D. Guu, J. K. G. Dhont, G. A. Vliegenthart, and M. P. Lettinga, J. Phys.: Condens. Matter **24**, 464101 (2012).
[40] J. Opdam, M. P. M. Schelling, and R. Tuinier, J. Chem. Phys. **154**, 074902 (2021).
[41] H. N. W. Lekkerkerker, W. C.-K. Poon, P. N. Pusey, A. Stroobants, and P. B. Warren, Europhys. Lett. **20**, 559 (1992).
[42] B. Widom, J. Chem. Phys. **39**, 2808 (1963).
[43] N. F. Carnahan and K. E. Starling, J. Chem. Phys. **51**, 635 (1969).
[44] V. F. D. Peters, M. Vis, H. H. Wensink, and R. Tuinier, Phys. Rev. E **101**, 062707 (2020).
[45] M. A. Cotter, Phys. Rev. A **10**, 625 (1974).
[46] H. Reiss, H. L. Frisch, and J. L. Lebowitz, J. Chem. Phys. **31**, 369 (1959).

[47]M. A. Cotter and D. E. Martire, J. Chem. Phys. **52**, 1902 (1970).
[48]M. A. Cotter and D. E. Martire, J. Chem. Phys. **52**, 1909 (1970).
[49]M. A. Cotter and D. E. Martire, J. Chem. Phys. **53**, 4500 (1970).
[50]M. F. Holovko and M. V. Hvozd, Condens. Matter Phys. **20**, 43501 (2017).
[51]Á. G. García, J. Opdam, R. Tuinier, and M. Vis, Chem. Phys. Lett. **709**, 16 (2018).
[52]J. Sambrook, E. F. Fritsch, and T. Maniatis, *Molecular Cloning: A Laboratory Manual*, 2nd ed. (Cold Spring Harbor Laboratory Press, 1989).
[53]S. A. Berkowitz and L. A. Day, J. Mol. Biol. **102**, 531 (1976).
[54]J. Tang and S. Fraden, Liq. Cryst. **19**, 459 (1995).
[55]Z. Dogic, "Liquid crystalline phase transitions in virus and virus/polymer suspensions," Ph.D. thesis, Brandeis University, 2000.
[56]E. Grelet and R. Rana, Soft Matter **12**, 4621 (2016).
[57]E. Grelet and S. Fraden, Phys. Rev. Lett. **90**, 198302 (2003).
[58]D. J. Pine, D. A. Weitz, P. M. Chaikin, and E. Herbolzheimer, Phys. Rev. Lett. **60**, 1134 (1988).
[59]Y. Mao, M. E. Cates, and H. N. W. Lekkerkerker, J. Chem. Phys. **106**, 3721 (1997).
[60]K. Yaman, C. Jeppesen, and C. M. Marques, Europhys. Lett. **42**, 221 (1998).
[61]R. Roth, J. Phys.: Condens. Matter **15**, S277 (2003).
[62]Y. Mao, M. E. Cates, and H. N. W. Lekkerkerker, Phys. Rev. Lett. **75**, 4548 (1995).
[63]I. Bodnár and W. D. Oosterbaan, J. Chem. Phys. **106**, 7777 (1997).
[64]R. Tuinier, Eur. Phys. J. E **10**, 123 (2003).
[65]M. Fasolo and P. Sollich, J. Chem. Phys. **122**, 074904 (2005).
[66]R. P. Sear and D. Frenkel, Phys. Rev. E **55**, 1677 (1997).
[67]P. B. Warren, Langmuir **13**, 4588 (1997).
[68]E. G. M. Pelssers, M. A. C. Stuart, and G. J. Fleer, Colloids Surf. **38**, 15 (1989).
[69]D. Kleshchanok and P. R. Lang, Langmuir **23**, 4332 (2007).
[70]M. Dijkstra, R. van Roij, and R. Evans, Phys. Rev. E **59**, 5744 (1999).